

Torque sharing function optimization for switched reluctance motor control using ant colony optimization algorithm

Dhiyaa Mohammed Ismael, Thamir Hassan Atyia

Department of Electrical Engineering, College of Engineering, University of Tikrit, Tikrit, Iraq

Article Info

Article history:

Received Jan 30, 2025

Revised Jun 21, 2025

Accepted Jul 23, 2025

Keywords:

Ant colony optimization
Motor drive optimization
Switched reluctance motor control
Torque ripple
Torque sharing function

ABSTRACT

Switched reluctance motors (SRMs) are gaining popularity in industrial and automotive applications due to their robust design, fault tolerance, and high torque density, particularly in wide-speed-range operations. However, SRM performance is often limited by torque ripple, speed oscillations, and inefficiencies, which can lead to mechanical stress, vibration, and acoustic noise. Addressing these challenges requires the effective optimization of control strategies. This study aims to enhance the performance of SRM drives by employing an ant colony optimization (ACO) algorithm to optimize the torque sharing function (TSF). The proposed method iteratively tunes TSF parameters to minimize torque ripple and improve speed stability under varying operating conditions. Simulation results demonstrate significant improvements: torque ripple is reduced from a range of -20 Nm to 10 Nm without optimization to below 10 Nm with ACO-based optimization. Similarly, current peaks decrease from 60 A to 5.5 A, ensuring smoother motor operation and enhanced efficiency. Comparative analysis confirms that the ACO-based TSF provides superior tracking of speed set points, reduced mechanical stress, and improved reliability, making it well-suited for high-performance applications in both industrial and automotive sectors.

This is an open access article under the [CC BY-SA](#) license.



Corresponding Author:

Thamir Hassan Atyia

Department of Electrical Engineering, College of Engineering, University of Tikrit

Tikrit, Iraq

Email: dr.thamir.atyia@tu.edu.iq

1. INTRODUCTION

Due to their superior design, robustness, and capacity to operate in challenging environments, switched reluctance motors (SRMs) have emerged as a competitive choice for modern industrial and automotive applications. They are ideal for applications requiring extended working ranges because of their inherent advantages, which include fault tolerance and high torque density. On the other hand, their torque generation is non-linear, which makes it difficult to provide effective and seamless control across a wide range of speeds. Torque ripple is a common problem in SRMs that requires modern management techniques for efficient mitigation since it can result in mechanical stress, vibration, and auditory noise. There have been several management solutions proposed to decrease the torque ripple in SRMs. Even though the torque sharing functions (TSFs) is frequently only applied at low to medium speeds, it is one of the most popular and successful techniques for lowering torque ripple. This study proposes an enhanced TSF to improve torque characteristics of SRMs over a wider speed range. The suggested method also improves motor efficiency by lowering the phase current's root mean square (RMS) value. Torque ripple reduction is an important area of research for SRMs because of its effects on the performance of motors, efficiency, and reliability. Many techniques have been put forth to enhance TSFs, each with unique approaches and drawbacks.

A genetic algorithm-based technique for altering commutation angles was presented in [1], which decreased torque ripple and Cu losses. The study also removes negative torque effects, which lower the average torque. Nevertheless, its application in quickly changing settings may be limited due to its reliance on GA parameters for convergence. A new TSF technique in [2] improves performance at high speeds by redefining TSF parameters to incorporate negative torque zones. The torque-speed characteristics and current dynamics are successfully enhanced by the technique.

Traditional TSFs for SRMs are designed to reduce torque ripple by shaping the phase current profile. However, conventional approaches such as linear, sinusoidal, and exponential TSFs do not account for real-time current dynamics and induced electromotive force (EMF), limiting their effectiveness in achieving precise torque control [3]. To enhance SRM performance, an online TSF method was introduced in [4], which dynamically adjusts the current reference based on real-time measurements. The current reference is updated using the fading phase current following the turn-off angle. The method ensures accurate torque production while minimizing copper losses. Several methods have been explored in [5] to reduce copper loss and torque ripple in motors with switching reluctance, particularly during commutation. Predictive torque control techniques have been widely studied for optimizing phase torque transitions and improving motor efficiency. Prior research has focused on refining cost functions and weight parameters to enhance control performance. However, existing methods still face challenges in achieving a balance between torque ripple suppression and copper loss reduction. Although this method significantly reduces torque ripple and improves operating efficiency, it may be less flexible in dynamic situations due to its reliance on static assessment indices.

Li *et al.* [6] presented an offline TSF method that makes use of TSF-based static flux linkage properties, showing little copper loss and a broad speed range. Even it works well in simulations, its offline nature makes it less flexible when operating circumstances change in real life. Ye *et al.* [7] presented a new extended-speed, low-ripple torque control method for SRM drives was proposed with an online TSF. The absolute values of the flux linkage rate change between the arriving and leaving phases determine the two operational modes. A proportional integral (PI) compensator is added to the torque reference to account for torque errors caused by insufficient current monitoring. Unlike traditional TSFs, our approach guarantees that the phase with the lowest absolute rate of change of flux linkage (ARCFL) determines the total torque. The system's superiority over traditional TSFs is confirmed by simulations testing using a 2.3 kW, 6000 rpm, 3-phase 12/8 SRM. This method significantly reduces ripples in torque and advances maximum torque-ripple-free speed by more than 10 times. The method relies on precise control of ARCFL, which may be challenging to implement in real-time under dynamic operating conditions. Increased computational requirements for implementing the PI compensator in real-time applications [8]. Addresses the major disadvantage of SRMs, high torque ripples, & by exploring an optimized torque control strategy based on TSFs. An improved conventional TSF and its associated online TSF are presented together with a changed current control method. This method greatly enhances torque-speed performance and torque ripple reduction. The optimization process is limited by its heavy reliance on system-specific factors.

Bober and Ferková [9] presented a TSF-based control of SRMs with the firing angle modulation (FAM) approach was presented. An off-the-shelf SRM-specific offline optimization process is presented, emphasizing integral square error, torque ripple, and motor efficiency. The FAM approach, which uses a finite element model (FEM), creates noticeably more torque ripple but is just as efficient as TSF. Ye *et al.* [10] presented using a Tikhonov factor, a torque ripple reduction offline TSF across a broad range of speeds is suggested to balance torque-speed performance with Cu loss. Its maximum torque-ripple-free speed is seven times faster than that of conventional TSFs. The method's offline nature limits its capacity to adjust to changes in real-time operations. Makwana *et al.* [11] presented an artificial neural network (ANN)-based procedure for SRMs. The method uses MATLAB Simulink to design and simulate the ANN, achieving satisfactory results. A novel approach to reduce the number of neurons for mapping magnetic characteristics is introduced, decreasing computational complexity without significantly affecting performance. The ANN design requires extensive training and accurate magnetic characteristic data, which might not be readily available [12]. Investigated mathematical modelling methods for SRMs, such as creating a MATLAB embedded function to map magnetic nonlinearity. As stated in [13], a hybrid TSF technique effectively addresses the issue of torque ripple in SRMs at high-speed re-profiling the increasing part of the entering phase torque to take into consideration for errors in outgoing phases. Additionally, by reducing the discrepancy between the requested and actual value of torque during high-speed operations, the overlap angle controller improves real-time torque monitoring capabilities. Simulation results validate that the hybrid TSF achieves significant torque ripple suppression compared to conventional TSFs. However, the method's reliance on real-time adaptation and computational resources could pose challenges in the implementation for resource-constrained systems.

Quraan *et al.* [14] presented an ITC strategy using a TSF to reduce ripple in torque in SRMs, especially at intermediate and high speeds. During the demagnetizing period, the suggested method predicts the outgoing phase torque and modifies the incoming phase torque appropriately to compensate for torque-tracking

inaccuracies. The method demonstrates a torque ripple reduction ranging from 10% to 45% and enhances efficiency through reduced copper losses, validated using finite element analysis. A limitation is the increased computational complexity associated with predictive control algorithms, which might impact real-time operation [15]. Focuses on enhancing the TSF method for SRMs to achieve higher operating speeds by minimizing the flux linkage change rate using genetic algorithm (GA) optimization. By refining known parameters and introducing a new optimization objective, the study demonstrates significant improvements in speed performance. Simulation outcomes authenticate the effectiveness of the approach. However, this research primarily emphasizes speed improvements, with limited attention to the potential impact on torque ripple or efficiency, making the analysis less comprehensive.

An optimization approach is described in [16] to identify the ideal parameters for sinusoidal TSF in SRMs, with an emphasis on start and overlap angles at different operational points. Several goal functions, including efficiency and torque ripple, are taken into account during the optimization process, which is conducted through simulations utilizing the finite element approach. The approach offers flexibility and diversity by generating a set of functions that are tailored for each operating point. However, the findings' generalizability to other SRM designs or operational settings would be limited by the study's dependence on the accuracy of finite element models. A unique TSF approach that divides the commutation process into two phases is presented in [17] to improve torque tracking performance in SRMs. The adaptive commutation approach guarantees better performance at various speeds by computing partition angles [18]. Provides an improved TSF with linear active disturbance rejection control (LADRC) and the modified coyote optimization algorithm (MCOA) to improve torque control in SRMs. While MCOA adjusts crucial factors, including turn-on and conduction angles, LADRC enhances anti-disturbance performance, and the piecewise TSF reduces torque ripple. Comparisons between simulation and experiment show that the scheme works healthier in terms of disturbance rejection and ripple decrease than traditional TSF techniques. However, the use of sophisticated optimization and control schemes adds complexity to the system, which may make practical implementation more difficult. Dowlatshahi *et al.* [19] presented that torque ripple compensation in SRMs is achieved by adapting standard TSFs to account for the nonlinear magnetic properties and torque pulsation mechanism. The proposed approach aims to enhance torque control. Further evaluation is required to determine its practical impact with greater accuracy. A TSF control technique for SRMs that maximizes torque per square ampere is used in [20] to improve motor efficiency and decrease torque ripple. Better torque tracking is achieved by the method by employing an online torque correction methodology and forecasting phase torque using real-time phase currents. Significant gains in torque ripple reduction over the cosine-type TSF technique are shown by simulation and experimental data.

Hamouda *et al.* [21] presented a new approach for SRMs to satisfy electric vehicle (EV) specifications like greater speed range, low torque ripple, and good efficiency was presented. Control parameters are adjusted using the particle swarm optimization (PSO) method, and torque tracking problems are fixed using a modified TSF. Simulation and finite element analysis validate the feasibility of the method across a broad speed range. However, adding PSO increases the computational complexity, which might cause issues for real-time EV applications. Two TSF-based methods for torque ripple reduction in SRMs were reported in their paper [22]-[24]. They matched the flux linkage model with a 4th-order Fourier series and computed torque error using a 6th-order polynomial. These strategies ensure precise torque tracking and ripple reduction, validated through simulation and digital signal processor (DSP)-based experimental implementation. While effective, the dependency on a detailed flux linkage model may limit the generalization of the approach to SRMs with different designs or operating conditions. A current-optimized TSF method with a quasi-proportional resonance (QPR) controller is offered in [25] to reduce torque ripple and Cu losses in SRMs. By dividing the operating regions based on torque-current ratios and incorporating inductance effects, the method achieves improved torque utilization and reduced current peaks. Experimental outcomes on a 3-phase 12/8 SRM confirm enhanced torque tracking and dynamic response. However, the complexity introduced by region-specific optimizations and QPR integration may increase design and implementation challenges. Dowlatshahi *et al.* [26] presented torque ripple minimization in SRMs by modifying conventional TSFs to account for phase inductance changes during commutation. This technique extends the region of constant torque and lowers peak phase currents at higher speeds by adjusting phase torque tracking errors among incoming and outgoing phases to keep constant resultant torque. Its efficacy is confirmed by real-time and simulation data for a 4 kW, 8/6 SRM. Nonetheless, the method's reliance on precise inductance modelling might limit its adaptability to SRMs with varying characteristics or converter limitations. A new approach combining direct torque control (DTC) with ant colony optimization (ACO) for proportional-integral-derivative (PID) parameter tuning is proposed to enhance the control of doubly fed induction motors (DFIMs) and is presented in [27]. The ACO-DTC approach optimizes PID gains using a cost function such as integral square error (ISE) to reduce torque ripple and speed overshoot. Improved system performance and robustness are demonstrated via real-time data on the dSPACE DS1104 platform. The variable-reluctance machine magnetization characteristics were presented in [28]. Table 1 shows the various TSF methods with their contribution & limitations inferred from the literature review.

Table 1. Summary of TSF-based methods with their key contribution and limitations

Ref	Method	Key contributions	Limitations
1	GA-based commutation angle adjustment	Reduced torque ripple and Cu losses	Limited in dynamic environments due to GA convergence dependency
2	New TSF technique	Improved performance at high speeds	Complexity due to negative torque zone handling
5	TSF static flux linkage offline	Low Cu loss, wide speed range	Offline nature limits real-time flexibility
6	Online TSF with ARCFL	High torque ripple reduction	High computational requirements for PI compensator
7	Optimized online TSF	Enhanced torque-speed and ripple reduction	System-specific dependency limits generalizability
8	TSF vs FAM approach	FAM is efficient but has more torque ripple	Offline optimization ignores real-world dynamics
9	Offline TSF with Tikhonov factor	Wide speed range, torque ripple reduction	Offline limits adaptability
12	Hybrid TSF approach	High-speed ripple suppression	High computational load in real-time
13	ITC strategy with TSF	10–45% ripple reduction	Complex predictive algorithm
14	GA-optimized TSF	High-speed performance improvement	Less focus on ripple and efficiency
15	Sinusoidal TSF optimization	Flexible for different operational points	Depends on accurate FEM
16	Two-phase TSF commutation	Better performance at various speeds	Implementation complexity
17	TSF with LADRC and MCOA	Superior ripple and disturbance control	Complex control methods
18	Adaptive TSFs with nonlinearity	Improved torque control	Incomplete details, unclear impact
21	Fourier + polynomial TSF models	Precise tracking and ripple reduction	Design-specific, limited generalization
22	Current-optimized TSF + QPR	Improved torque and dynamic response	Design complexity
23	TSF with phase inductance adjustment	Extended constant torque region	Needs precise inductance modeling

The literature states that existing TSFs and optimization methods for SRMs have a number of shortcomings, including an inability to respond in real time, an excessive amount of computer complexity, and an inability to properly eliminate torque ripple at high speeds. Current approaches frequently fail to manage dynamic torque control under changing load, speed conditions, and leading to suboptimal performance. Furthermore, their impact on lowering acoustic noise and vibration has not been well studied, and many methods fall short in effectively optimizing current profiles, which increases copper losses. Moreover, most methods are system-specific and do not scale or generalize to other SRM configurations. To resolve the issues, this paper offers an optimum TSF approach based on the ACO algorithm. The TSF is fundamental for effectively dispersing torque across the motor phases, which lowers ripple and enhances overall performance. By using the ACO algorithm, the proposed method ensures optimal TSF parameter tuning, expanding the motor's speed range, and improving dynamic responsiveness. Simulation findings show that the ACO-based TSF approach is successful in increasing the reliability and efficiency of SRM drives for high-performance applications.

Contribution of the paper: Develop an optimized TSF strategy for minimizing torque ripple in SRM drives across a wide speed range; implement the ACO algorithm for fine-tuning TSF parameters, for current control ensuring improved torque production and dynamic performance; validate the effectiveness of the proposed ACO-based TSF strategy through simulation, comparing its performance in terms of torque ripple reduction, extended speed capability, and motor performance.

Organization of the paper, the paper is divided into the following sections: i) Section 2 introduces the SRM torque characteristics and sinusoidal TSF; ii) Section 3 details the proposed 6/4 SRM; iii) Section 4 explains how to tune the PI controller using MGO in the speed controller; iv) Section 5 explains how to implement ACO control for TSF to reduce torque ripples and achieve effective speed control; v) Section 6 displays the results and discussion of the suggested scheme; and vi) Section 7 concludes and outlines the future scope of the work.

2. TORQUE SHARING FUNCTIONS

2.1. Switched reluctance motor torque characteristics

The rotor position and current cause a nonlinear change in the SRM flux characteristic. The phase voltage is given by:

$$v_j = R_j i_j + \frac{d\lambda_j(i, \theta)}{dt} \quad j = 1, 2, \dots, m \quad (1)$$

where, v_j is the Terminal voltage, R_j is Resistance, i_j is phase current, $\lambda_j(i, \theta)$ is the Flux linkage of j-th phase winding, $\theta(t)$ is the Rotor position as a function of time, and m is the total number of stator phases. Depending on the partial derivative of the co-energy, the instantaneous torque is expressed by (2).

$$T_j(i, \theta) = \frac{\partial W_j^c(i, \theta)}{\partial \theta} \quad (2)$$

Here i is Constant, where $W_j^c(i, \theta)$ is provided by (3).

$$W_j^c(i, \theta) = \int_0^{i_j} \lambda_j(i, \theta) di_j \quad (3)$$

The total phase torques equal the total instantaneous torque in this case, where θ is constant.

$$T_e(i, \theta) = \sum_{j=1}^m T_j(i, \theta) \quad (4)$$

The entire instantaneous torque is integrated to determine the average torque.

$$T_{avg} = \frac{1}{\theta_r} \int_0^{\theta_r} T_e d\theta \quad (5)$$

The following is how the RSM current affects the copper losses:

$$I_{RMS} = \sqrt{\frac{1}{\theta_r} \int_0^{\theta_r} i_j^2 d\theta} \quad (6)$$

As a proportion of the average torque at steady-state operation, the torque ripple is the difference between the maximum ($T_{instmax}$) and minimum instantaneous torque ($T_{instmin}$).

$$\text{Torque ripple} = \left| \frac{T_{instmax} - T_{instmin}}{T_{avg}} \right| \times 100\% \quad (7)$$

The quantity of torque ripple during operation is influenced by the SRM's torque–current–position properties. In this work, the static DC test was used to experimentally determine $\lambda(i, \theta)$. The SRM's stator phase current was raised during the DC test trials. After that, analytical calculations were used to determine $W_j^c(i, \theta)$ and $T_j(i, \theta)$.

2.2. Torque sharing function

2.2.1. Sinusoidal TSF

The following is a model of the sinusoidal TSF. The three angles that make up the TSFs are turn on, overlap, and turn off. Figure 1 shows the sinusoidal TSF profile. The torque regard of T_j is specified as follows during the commutation:

$$T_j = \begin{cases} T_j^* \cdot f_{rise}^{TSF}, & (\theta_{on}) \leq \theta_j < (\theta_{on} + \theta_{ov}) \\ T^*, & (\theta_{on} + \theta_{ov}) \leq \theta_j < (\theta_{off}) \\ T_j^* \cdot f_{fall}^{TSF}, & (\theta_{off}) \leq \theta_j < (\theta_{on} + \theta_{ov}) \\ 0, & \text{otherwise} \end{cases} \quad (8)$$

where, T_j^* is the desired torque for phase j at rotor position θ_j . T^* is the total reference torque required from the motor, T_j^* is the maximum torque contribution from phase j , f_{rise}^{TSF} & f_{fall}^{TSF} is the rising & falling position of TSF. θ_{on} , θ_{off} & θ_{ov} are the turn on, turn off & overlap angle. Where the turn on, turn off, and overlapping angles are denoted by θ_{on} , θ_{off} , and θ_{ov} , respectively. The rising TSF, or incoming phase f_{rise} , is defined as (9).

$$f_{rise} = \frac{1}{2} - \frac{1}{2} \cos \left(\frac{\pi}{\theta_{ov}} (\theta_j - \theta_{on}) \right) \quad (9)$$

The lowering TSF contradicts the outgoing phase f_{fall} .

$$f_{fall} = \frac{1}{2} - \frac{1}{2} \cos \left(\frac{\pi}{\theta_{ov}} (\theta_j - \theta_{off}) \right) \quad (10)$$

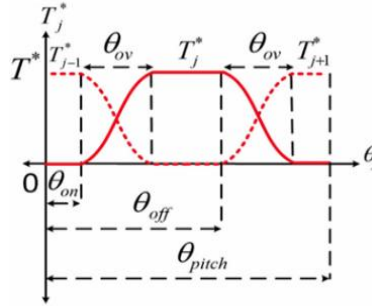


Figure 1. Representation of sinusoidal TSF [1]

3. PROPOSED MODEL PARAMETERS

The geometrical dimensions and turn details of the selected 60 kW, 6/4 SRM are provided in Table 2. Table 3 summarizes the model parameters of the SRM. The magnetization characteristics of the SRM are shown in Figure 2.

Table 2. Geometry and turn details of SRM

Parameter	Value
Shaft radius	0.0143
Rotor radius (back iron)	0.034
Radius behind rotor poles	0.041
Rotor pole base width	0.032
Rotor radius at airgap	0.055
Airgap thickness G	0.0002
Stator radius at airgap R,	0.0552
Stator pole tip radius	0.082
Outer radius Ro	0.1
Effective axial length d	0.3
Rotor pole angle	45
Stator pole angle	32
Total rotor poles N,	4
Coil turns per pole	13

Table 3. Model parameters

Parameter	Value
Position where rotor and stator reach maximum overlap (rad)	6.5°
Position between θ_1 & θ_2	12.83°
Position where the rotor and stator reach zero overlap (rad)	28.5°
Rotor gap arc length to stator pole dimension	1.40
Rotor pole undercut to the gap between rotor poles	0.486
factor for third dimension correction	1.125
Inductance Lmax	23.62 mH
Inductance Lcorner	1.19 mH
Inductance Lmin	0.67 mH
Magnetic coefficient (a1)	439.6 mWb
Magnetic coefficient (a2)	43.96 mWb
Magnetic coefficient (a3)	117.7 μ H

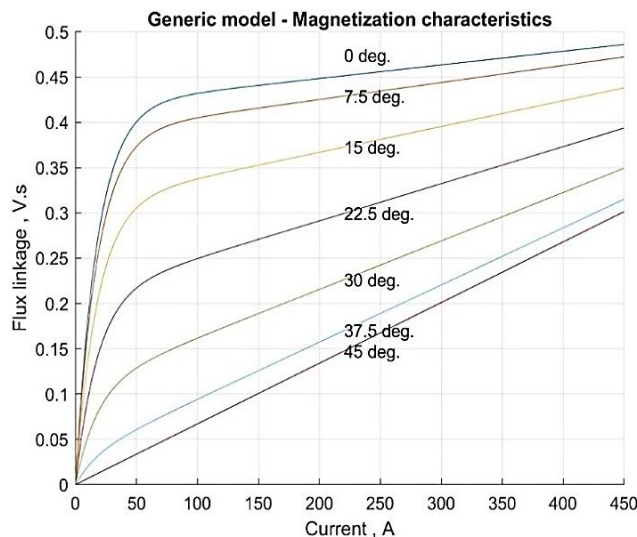


Figure 2. Magnetization characteristics of the SRM

4. PI CONTROLLER TUNING USING MGO IN SRM

The speed controller is a critical component in the simulation that ensures the SRM operates at the desired speed by adjusting its torque output. Input to the speed controller is reference (N_{ref}), which represents

the target speed at which the motor is expected to run. The actual rotor speed, measured in real time (N_r), is fed back into the controller to compare with the reference speed. The output of the controller is a speed error signal, which indicates the variation between the reference and actual speeds. This closed-loop feedback mechanism ensures the system adapts to disturbances or variations in load to maintain the desired speed. The PI controller processes the speed error information and then outputs the torque reference signal (T_{ref}), which is needed to operate the motor. The proportional gain of the controller reacts to the magnitude of the speed error and quickly corrects errors. On the other hand, the integral gain treats any steady-state errors that could be missed by the proportional term by accumulating the error over time. Together, these components decrease speed errors and ensure the SRM runs smoothly. The PI controller is fine-tuned using the mountain gazelle optimizer (MGO) technique. MGO is a natural optimization method that efficiently determines the optimal values of K_p and K_i by mimicking the strategic movements and energy-efficient behaviors of mountain gazelles. MGO ensures that the speed controller achieves better tracking accuracy and dynamic response while minimizing overshoot, settling time, and steady-state error through the optimization of the controller gains. This improved PI-MGO controller not only improves the motor's speed regulation capabilities across a range of operating conditions, but it also reduces torque ripple and increases system efficiency. The PI-MGO controller generates the output torque reference signal (T_{ref}), which is sent to the TSF module.

5. ACO CONTROL FOR TSF

The speed w^* and the commanded reference torque T^* are the inputs. By using a TSF block to intelligently divide the input torque between motor phases, the phase torque signal T_{ph}^* is produced. Every phase torque signal is then translated into its subsequent reference current profile i^* , and by accurately tracking this current using a hysteresis controller, the torque is indirectly controlled. After counting the remaining portion of the rotor position (-30 to 0), the model uses the torque and current lookup tables. The current lookup table $i(\lambda, \theta)$ is produced by inverting the pole flux data in Figure 3. The waveforms for phase current (i_{ph}) and total electromagnetic torque (T_e) are the model's outputs. The sinusoidal TSF, one of the most widely utilized TSF kinds, is employed in this method because it provides the lowest rate of flux linkage change with the least amount of current. Figure 3 shows how to use ACO Control to control 6/4 SRM.

$$TSF(\theta) = \begin{cases} 0, (0 \leq \theta < \theta_{on}) \\ \frac{T^*}{2} - \frac{T^*}{2} \cos \frac{\pi}{\theta_{ov}} (\theta - \theta_{on}), (\theta_{on} \leq \theta < \theta_1) \\ T^*, (\theta_{on} + \theta_{ov} \leq \theta < \theta_{off}) \\ \frac{T^*}{2} + \frac{T^*}{2} \cos \frac{\pi}{\theta_{ov}} (\theta - \theta_{off}), (\theta_{off} \leq \theta < \theta_2) \\ 0, (\theta_{off} + \theta_{ov} \leq \theta < \theta_p) \end{cases} \quad (11)$$

Where θ_{on} , θ_{off} , θ_{ov} , θ_p are the switch-on, switch-off, overlap, and rotor pitch angles. The overlap angle is subjected to (12).

$$\theta_{ov} \leq \frac{\theta_p}{2} - \theta_{off} \quad (12)$$

By carefully choosing the overlap angle and switch-on angle, the TSF displayed in the above figure may be maximized. In this investigation, ACO was used. To minimize the ripple of the torque and the RMS value of the phase current while maintaining a reasonable average out torque, the optimum values for control variables are selected using the proposed ACO [26].

5.1. Formulation of objective function

The optimization issue is stated (13)-(15):

$$F = w_1(T_{max} - T_{min}) + w_2(I_{rms}) \quad (13)$$

$$T_{ave} = \sigma T^* \quad (14)$$

$$\theta_{ov} \leq \frac{\theta_p}{2} - \theta_{off} \quad (15)$$

where T_{max} , T_{min} and T_{ave} are the output torque (T_e) waveform's highest, minimum, and average values, respectively; w_1 and w_2 are weighting factors; I_{rms} is the phase current's RMS value; and σ is a scaling factor

that defines the lowest permitted T_{ave} as a percentage of the requested torque T^* . In this study, σ falls between 0.85 and 0.95, while w_1 and w_2 are set to 0.1812 and 0.3791, respectively.

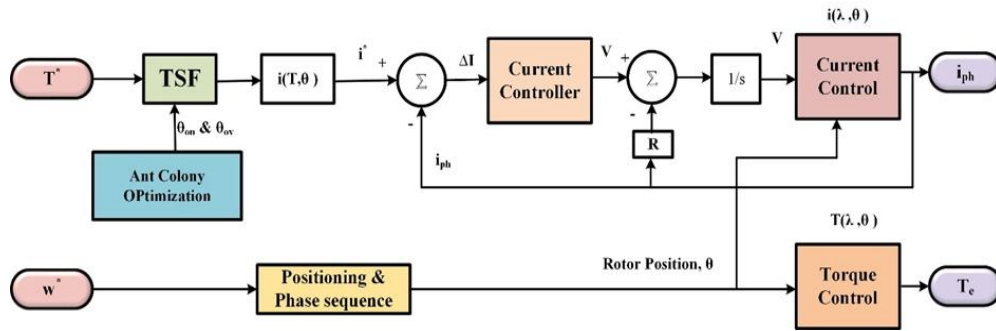


Figure 3. Control of 6/4 SRM using ACO control

5.2. Step-by-step algorithm for ACO

The ACO algorithm was implemented in MATLAB, where each ant represents a potential solution (a set of parameter values), and the pheromone matrix guides the search towards promising regions of the solution space. The number of nodes for each parameter was set to 1000 to ensure fine resolution in the parameter search space. The algorithm uses pheromone trail updating and evaporation to balance exploration and exploitation.

The selection of ACO parameters in this study includes the number of ants ($NA = 10$), pheromone evaporation rate ($\rho = 0.7$), and weighting factors ($\alpha = 0.8$, $\beta = 0.2$) were guided by empirical tuning and supported by existing literature. These values were chosen after conducting preliminary experiments to balance solution quality and computational efficiency. A moderate number of ants ensured sufficient search diversity without incurring excessive computational overhead. The evaporation rate was set at 0.7 to retain useful solution information while allowing exploration of new paths. The weighting parameters were set to emphasize pheromone influence (α) over heuristic information (β), aligning with the nature of the control problem where prior solution feedback is more critical than direct heuristics.

5.2.1. Implementation

This section presents the step-by-step implementation of the ACO algorithm, starting from parameter initialization and ending with the final system performance evaluation:

- a) Initialize ACO parameters
 - Specify a number of iterations, the number of ants, and other parameters related to the method, including the evaporation rate, alpha (α), beta (β), number of variables, lower and upper bounds, and number of nodes.
 - Initialize the pheromone matrix (T) with a small positive value (eps) and create placeholders for various variables such as ant positions, costs, and probabilities.
- b) Generate nodes
 - Divide the parameter search space into discrete nodes, equally spaced between the lower and upper bounds for each parameter. These nodes represent potential solutions to be explored by the ants.
- c) Start iteration loop
 - For each iteration, calculate the probability of selecting each node for each parameter based on the pheromone levels and heuristic values (inversely proportional to the nodes' values).
- d) Tour construction by ants
 - For each ant, determine its path (i.e., parameter values) by selecting nodes probabilistically:
 - Generate a random number to simulate a roulette wheel selection.
 - Accumulate probabilities for each node until the sum exceeds to choose the corresponding node index.
- e) Evaluate cost function
 - Use the selected parameter values to compute the cost for each ant. This step involves running a cost function that evaluates the excellence of chosen parameters created on a specific system, indicating performance, such as errors in speed and current.
- f) Update the best solution
 - Identify the ant with the minimum cost and its corresponding parameters. If the current best solution is worse than the previous iteration's best, retain the previous best solution (elitism).

- g) Pheromone update
 - Calculate the change in pheromone levels (ΔT) for each node based on the costs of the ants:
 - Nodes visited by better-performing ants receive higher pheromone increments.
 - Update the pheromone matrix (T) by combining the current levels and the newly calculated changes, scaled by the evaporation rate (ρ).
- h) Iterative optimization
 - Store the best cost and parameter values for the current iteration.
 - Plot the convergence of the cost over iterations for visualization.
- i) Simulation and system evaluation
 - Extract the optimized parameters (k_e , k_{ce}) from the best-performing ant.
 - Assign these parameters to the simulation environment (e.g., a Simulink model) to simulate the system's performance over a defined time period.
 - Compute performance metrics (e.g., speed and current errors) based on simulation results.
- j) Compute final fitness value
 - Calculate the fitness value as a weighted sum of the performance metrics (e.g., speed and current errors).
 - This value determines the quality of the selected parameters and provides feedback to guide the algorithm in subsequent iterations.
- k) End the algorithm
 - After completing the target value of epochs, return the optimized parameters and the corresponding fitness value.

Following these procedures, the ACO algorithm iteratively improves the system's performance by optimizing the parameters through collective ant behavior, probabilistic decision-making, and pheromone reinforcement mechanisms. Figure 4 presents the flow diagram for the suggested system using the ACO method.

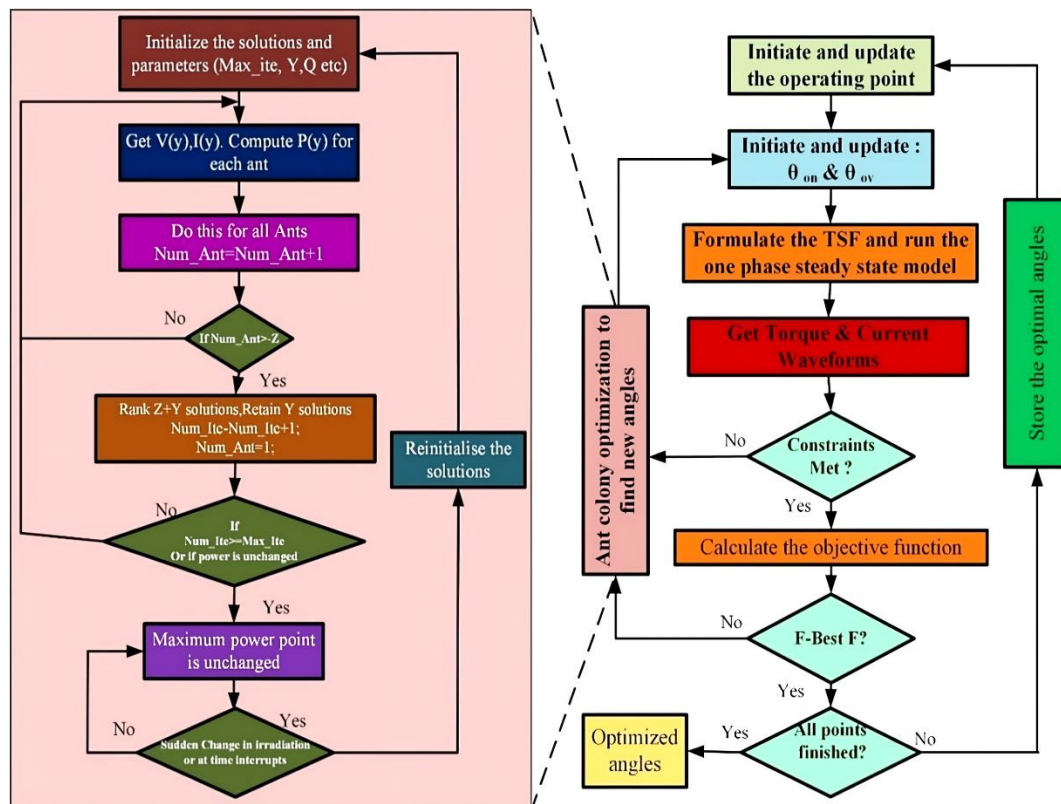


Figure 4. Flow diagram for the suggested system utilizing the ACO method

6. RESULTS & DISCUSSION

The suggested method's outcomes are examined both with and without optimization as follows:

6.1. Without optimization

6.1.1. Constant speed

During this operation, the system is operated at a constant speed; Figure 5 represents the torque & speed obtained during constant speed. The torque varies between -20 Nm and 10 Nm, while the speed exhibits oscillations with significant ripple content. Figure 6 represents the current without optimization during constant speed conditions; here, the maximum current is around 60 A.

6.1.2. Varying speed

During this condition, the system is operated at variable speed, and the torque & the current are denoted in Figure 7. In this condition, the oscillation is more in torque & speed; the speed is subjected to oscillations & torque has higher ripple content. The current during varying speed without oscillation is represented in Figure 8. Here are more current ripples. The maximum peak current appears in different instances.

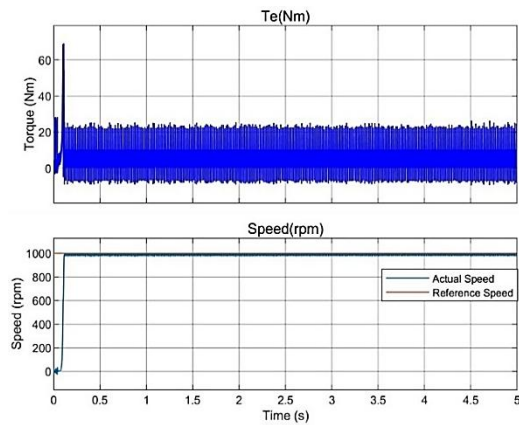


Figure 5. Constant speed and torque without optimization

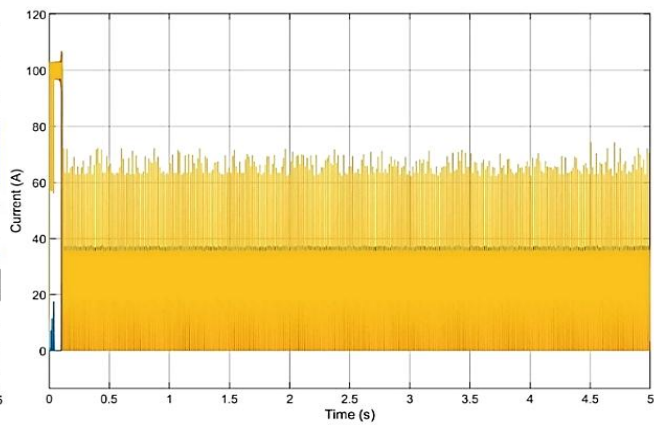


Figure 6. Current without optimization during constant speed

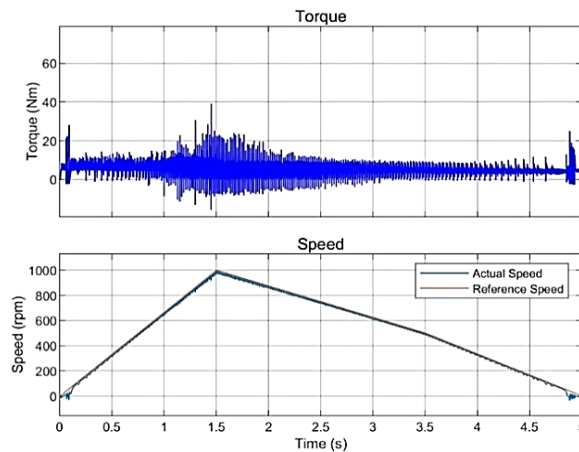


Figure 7. Varying speed and torque without optimization

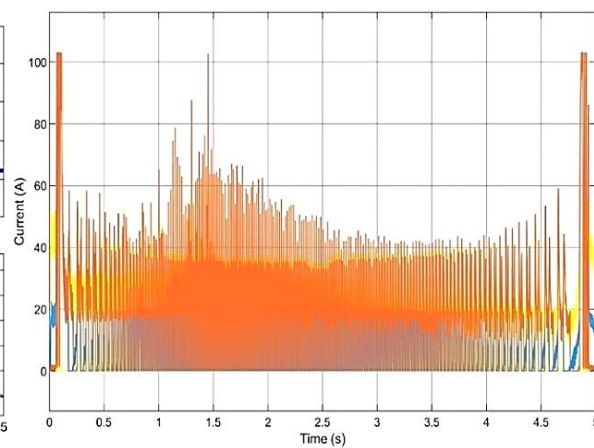


Figure 8. Current without optimization during varying speeds

6.2. With ACO Optimization

6.2.1. Constant speed

During this condition, ACO is implemented to tune the control variables; thereby, the torque ripple & the oscillation in the speed are minimized. Figure 9 represents the constant speed & torque with optimization. The torque is below 10 Nm, and the ripples are very low. The current obtained during constant speed with optimization is presented in Figure 10, the maximum current obtained is 5.5 A.

6.2.2. Varying speed

During this condition, the speed varied; the torque and speed are represented in Figures 11 and 12. The torque obtained is 10 Nm. The current is around 5.5 A.

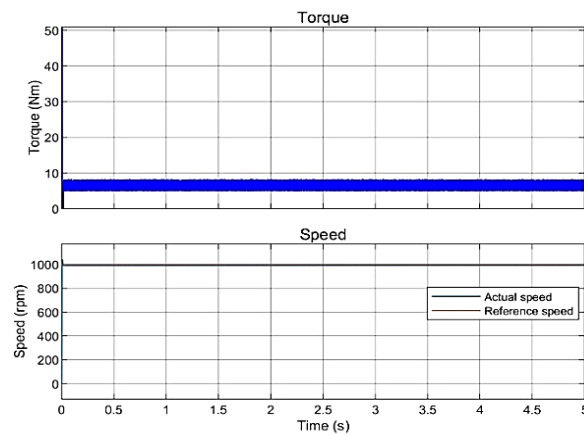


Figure 9. Constant speed and torque with ACO

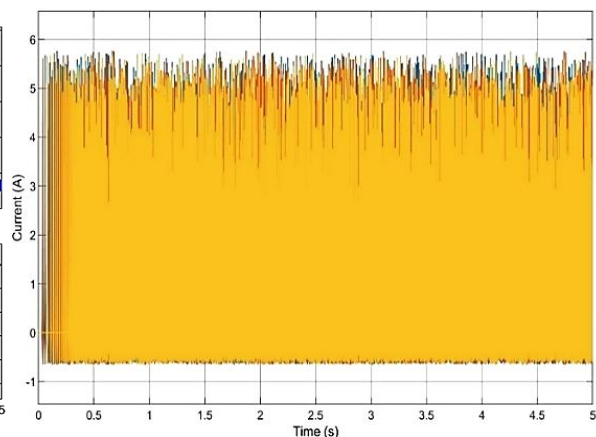


Figure 10. Current with optimization during constant speed

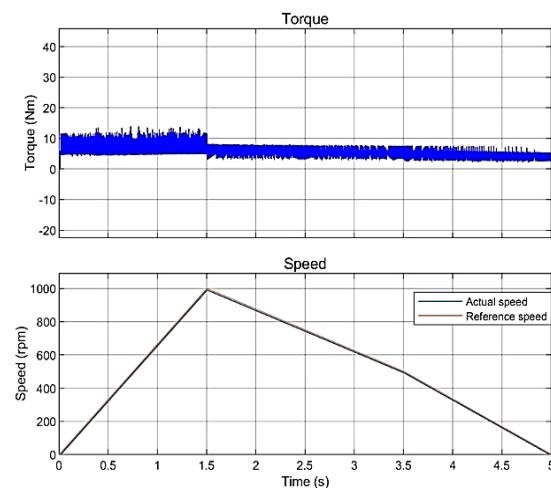


Figure 11. Varying speed and torque with ACO

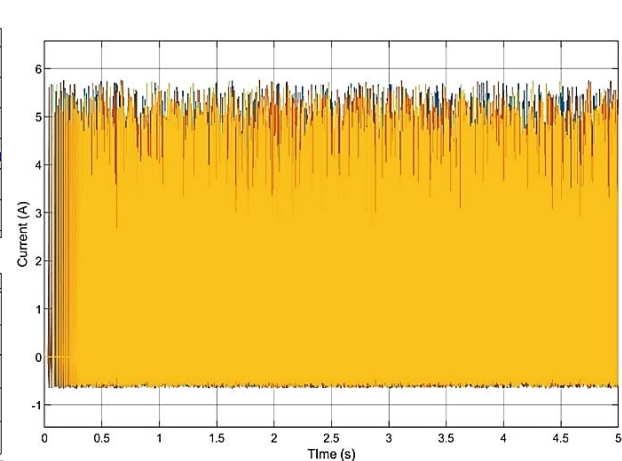


Figure 12. Current with optimization during varying speeds

7. COMPARATIVE ANALYSIS

The comparison of speed with and without oscillations is represented in Figure 13. The speed without optimization is subjected to more ripple with 15 V, whereas the speed after optimization is smooth and tracks the set-point value effectively using ACO. The comparison of varying speed with and without oscillations is demonstrated in Figure 14. The speed without optimization is subjected to more ripple with 20 V, whereas the speed after optimization is smooth and tracks the set-point value effectively using ACO.

Figure 15 shows the comparison of torque during constant speed; here, the comparative analysis clearly depicts that the torque ripple is more without optimization. Here, the ripple is from -10 to 20 Nm, whereas the torque with optimization has very few ripples & improves the performance of the motor operation. In Figure 16, the peak torque is obtained without optimization from -15 to 40 Nm, whereas the torque with optimization has very few ripples & improves the performance of the motor operation. Table 4 shows the comparison between the suggested ACO and GA & PSO.

Table 4 compares the effectiveness of GA, PSO, and ACO methods in reducing torque ripple in SRMs under both constant and variable speed conditions. Among the three, ACO demonstrates the best performance with the lowest torque ripple, 0.41% at constant speed and 0.86% under variable speed, indicating superior

smoothness and control. PSO also performs well, showing moderate ripple values of 1.84% and 2.68%, while GA records the highest ripple at 2.11% and 2.94%. This comparison highlights ACO as the most effective technique for minimizing torque ripple across varying operating conditions.

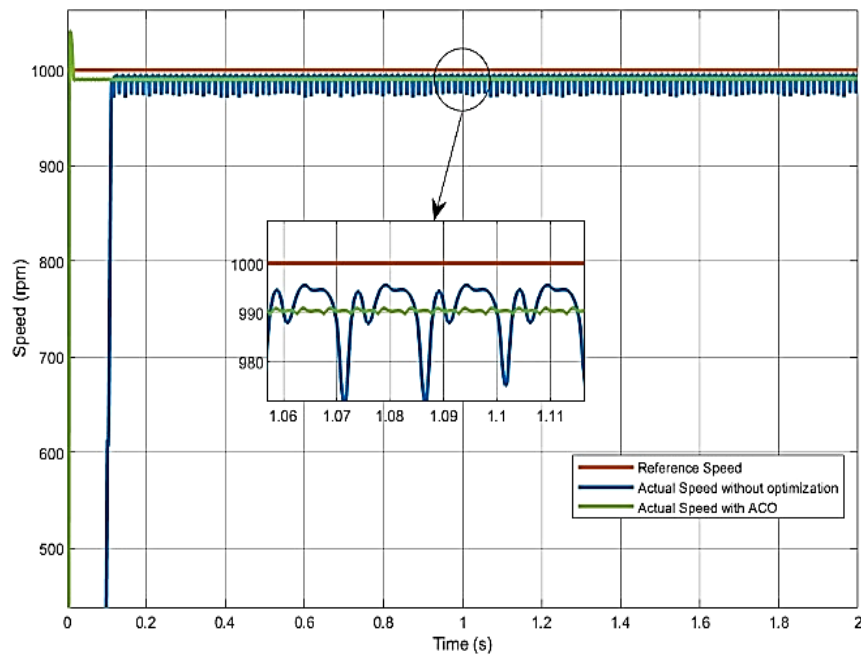


Figure 13. Comparison during constant speed operation

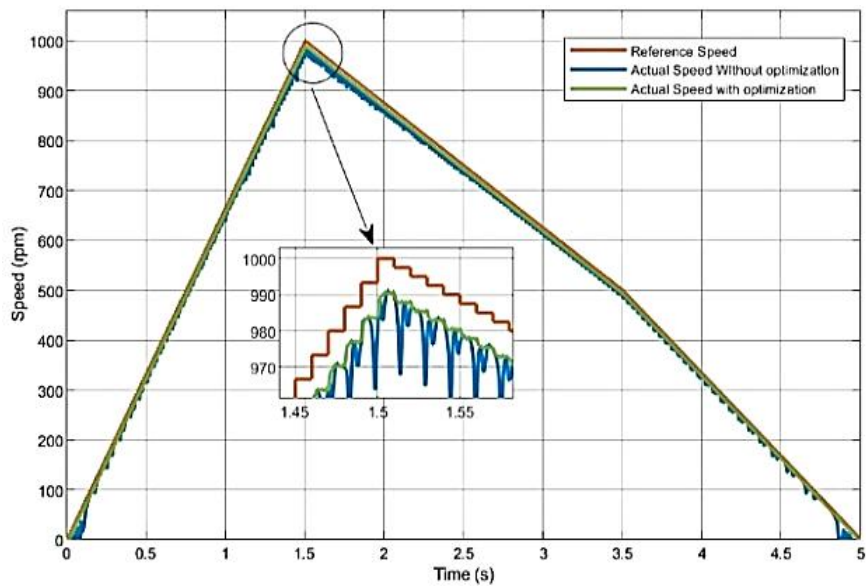


Figure 14. Comparison during variable speed operation

Table 4. Comparison of GA, PSO, and ACO methods

Method	% Torque ripple	
	Constant speed	Variable speed
GA	2.11	2.94
PSO	1.84	2.68
ACO	0.41	0.86

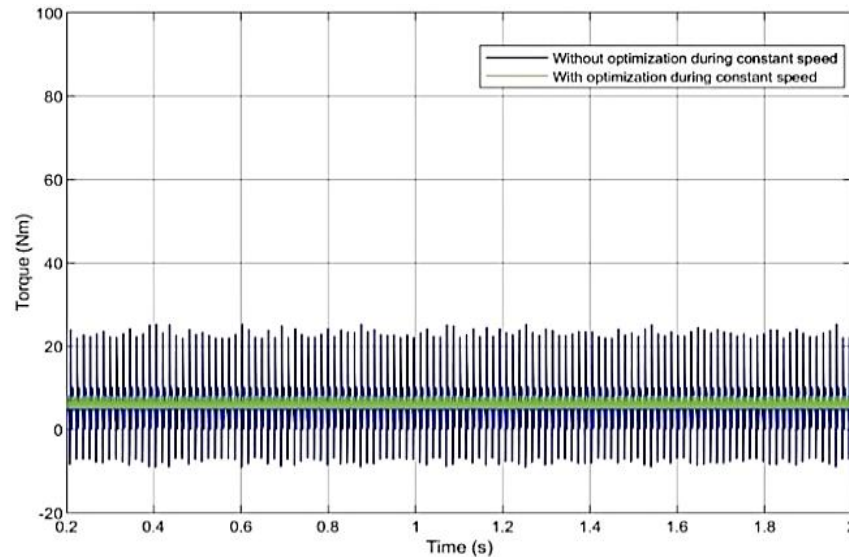


Figure 15. Torque comparison at constant speed

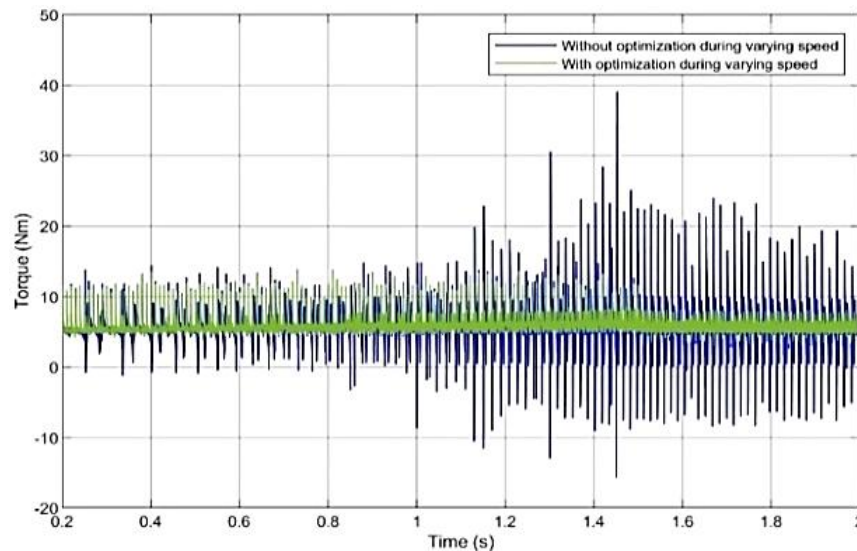


Figure 16. Torque comparison at varied speed

8. CONCLUSION

The study demonstrates the effectiveness of an optimized TSF strategy utilizing the ACO algorithm to enhance the performance of SRM drives across extended speed ranges. The results reveal that the ACO-based optimization significantly reduces torque ripple and minimizes speed oscillations during both constant and varying speed operations. Without optimization, the torque and speed profiles exhibit substantial oscillations, with torque fluctuating between -20 Nm and 10 Nm, and current peaking at approximately 60 A. Conversely, the implementation of the ACO algorithm achieves smoother torque and speed characteristics, reducing torque ripple below 10 Nm and current peaks to just 5.5 A. This marked improvement translates to enhanced motor efficiency and reduced mechanical stress, vibration, and acoustic noise. Comparative analysis further highlights that the optimized approach ensures better tracking of set speed points and minimizes the variation in torque, providing a more reliable and stable motor operation. These findings affirm the potential of the ACO-based TSF in advancing SRM drive applications, making them suitable for high-performance requirements in industrial and automotive sectors.

Future research could focus on implementing real-time ACO-based TSF optimization for SRM drives to adapt dynamically to varying operational conditions. Exploring hybrid optimization techniques combining ACO with other algorithms may yield further improvements in performance. Additionally, extending the study

to experimental setups with hardware-in-the-loop (HIL) systems could validate proposed method's applicability in practical scenarios, ensuring robust and adaptive control for diverse industrial and automotive applications.

ACKNOWLEDGEMENT

The authors greatly appreciate the support of Electrical Engineering Department, Tikrit University Iraq.

FUNDING INFORMATION

The authors received no financial support for the research, authorship, and/or publication of this article.

AUTHOR CONTRIBUTIONS STATEMENT

This journal uses the Contributor Roles Taxonomy (CRediT) to recognize individual author contributions, reduce authorship disputes, and facilitate collaboration.

Name of Author	C	M	So	Va	Fo	I	R	D	O	E	Vi	Su	P	Fu
Dhiyaa Mohammed Ismael		✓	✓	✓	✓	✓		✓	✓	✓	✓		✓	
Thamir Hassan Atyia	✓	✓		✓	✓		✓	✓	✓	✓		✓	✓	

C : **C**onceptualization

M : **M**ethodology

So : **S**oftware

Va : **V**alidation

Fo : **F**ormal analysis

I : **I**nterpretation

R : **R**esources

D : **D**ata Curation

O : **O**riginal Draft

E : **E**diting

Vi : **V**isualization

Su : **S**upervision

P : **P**roject administration

Fu : **F**unding acquisition

CONFLICT OF INTEREST STATEMENT

The authors declare no potential conflicts of interest with respect to the research, authorship, and/or publication of this article.

DATA AVAILABILITY

Data availability is not applicable to this paper as no new data were created or analyzed in this study.




REFERENCES

- [1] O. Üstün and M. Önder, "An improved torque sharing function to minimize torque ripple and increase average torque for switched reluctance motor drives," *Electric Power Components and Systems*, vol. 48, no. 6–7, pp. 667–681, 2020, doi: 10.1080/15325008.2020.1797939.
- [2] C. Choi, S. Kim, Y. Kim, and K. Park, "A new torque control method of a switched reluctance motor using a torque-sharing function," *IEEE Transactions on Magnetics*, vol. 38, no. 5, pp. 3288–3290, 2002, doi: 10.1109/TMAG.2002.802295.
- [3] Z. Xia, G. Fang, D. Xiao, A. Emadi, and B. Bilgin, "An online torque sharing function method involving current dynamics for switched reluctance motor drives," *IEEE Transactions on Transportation Electrification*, vol. 9, no. 1, pp. 534–548, 2022, doi: 10.1109/TTE.2022.3183171.
- [4] W. Ye, Q. Ma, and P. Zhang, "Improvement of the torque-speed performance and drive efficiency in an SRM using an optimal torque sharing function," *Applied Sciences*, vol. 8, no. 5, p. 720, 2018, doi: 10.3390/app8050720.
- [5] L. Sheng, G. Wang, Y. Fan, J. Liu, D. Liu, and D. Mu, "An improved direct predictive torque control for torque ripple and copper loss reduction in SRM drive," *Applied Sciences*, vol. 13, no. 9, p. 5319, 2023, doi: 10.3390/app13095319.
- [6] H. Li, B. Bilgin, and A. Emadi, "An improved torque sharing function for torque ripple reduction in switched reluctance machines," *IEEE Transactions on Power Electronics*, vol. 34, no. 2, pp. 1635–1644, 2018, doi: 10.1109/TPEL.2018.2835773.
- [7] J. Ye, B. Bilgin, and A. Emadi, "An extended-speed low-ripple torque control of switched reluctance motor drives," *IEEE Transactions on Power Electronics*, vol. 30, no. 3, pp. 1457–1470, 2014, doi: 10.1109/TPEL.2014.2316272.
- [8] R. Hari Krishnan and F. M. Fernandez, "Improved online torque-sharing-function based low ripple torque control of switched reluctance motor drives," in *Proceedings IEEE PEDES*, pp. 1–6, 2016, doi: 10.1109/PEDES.2016.7914374.
- [9] P. Bober and Ž. Ferková, "Comparison of an off-line optimized firing angle modulation and torque sharing functions for switched reluctance motor control," *Energies*, vol. 13, no. 10, p. 2435, 2020, doi: 10.3390/en13102435.
- [10] J. Ye, B. Bilgin, and A. Emadi, "An offline torque sharing function for torque ripple reduction in switched reluctance motor drives," *IEEE Transactions on Energy Conversion*, vol. 30, no. 2, pp. 726–735, 2015, doi: 10.1109/TEC.2014.2383991.
- [11] J. A. Makwana, P. Agarwal, and S. P. Srivastava, "ANN based sensorless rotor position estimation for the Switched Reluctance Motor," in *Proceedings IEEE NUIConE*, pp. 1–6, 2011, doi: 10.1109/NUIConE.2011.6153281.
- [12] J. A. Makwana, P. Agarwal, and S. P. Srivastava, "Modeling and simulation of switched reluctance motor," in *Advances in Systems, Control and Automation*, pp. 545–558, 2018, doi: 10.1007/978-981-10-4762-6_52.




- [13] F. Al-Amyal and L. Számel, "Research on novel hybrid torque sharing function for switched reluctance motors," *IEEE Access*, vol. 10, pp. 91306–91315, 2022, doi: 10.1109/ACCESS.2022.3202296.
- [14] L. Al Quraan, A. L. Saleh, and L. Szamel, "Indirect instantaneous torque control for switched reluctance motor based on improved torque sharing function," *IEEE Access*, 2024, doi: 10.1109/ACCESS.2024.3355389.
- [15] J. Fan and Y. Lee, "Extending maximum speed of torque sharing function method in switched reluctance motor," in *Proceedings. IEEE ICECCE*, pp. 1–5, 2021, doi: 10.1109/ICECCE52056.2021.9514235.
- [16] Ž. Ferková and P. Bober, "An off-line optimization of torque sharing functions for switched reluctance motor control," in *Proceedings IEEE ECMSM*, pp. 1–4, 2021, doi: 10.1109/ECMSM51310.2021.9468872.
- [17] R. Yang, X. Wang, Z. Huang, and Y. Ma, "Torque ripple minimization control of switched reluctance motor based on online torque sharing function," *IEEE Transactions on Power Electronics*, 2024, doi: 10.1109/TPEL.2024.3501574.
- [18] L. Feng, X. Sun, Z. Yang, and K. Diao, "Optimal torque sharing function control for switched reluctance motors based on active disturbance rejection controller," *IEEE/ASME Transactions on Mechatronics*, vol. 28, no. 5, pp. 2600–2608, 2023, doi: 10.1109/TMECH.2023.3240986.
- [19] M. Dowlatshahi, S. M. S. Nejad, and J. W. Ahn, "Torque ripple minimization of switched reluctance motor using modified torque sharing function," in *Proceedings IEEE ICEE*, pp. 1–6, 2013, doi: 10.1109/IranianCEE.2013.6599580.
- [20] X. Zhang, Y. Mao, X. Sun, L. Feng, and Y. Xiong, "torque online correction control of switched reluctance motor based on optimized torque sharing function," *IEEE Transactions on Energy Conversion*, 2024, doi: 10.1109/TEC.2024.3370741.
- [21] M. Hamouda, A. A. Menaem, H. Rezk, M. N. Ibrahim, and L. Számel, "An improved indirect instantaneous torque control strategy of switched reluctance motor drives for light electric vehicles," *Energy Reports*, vol. 6, pp. 709–715, 2020, doi: 10.1016/j.egy.2020.11.142.
- [22] T. Chen and G. Cheng, "Comparative investigation of torque-ripple suppression control strategies based on torque-sharing function for switched reluctance motor," *CES Transactions on Electrical Machines and Systems*, vol. 6, no. 2, pp. 170–178, 2022, doi: 10.30941/CESTEMS.2022.00023.
- [23] D. M. Ismael and T. H. Atyia, "Comparative evaluation of speed control techniques for switched reluctance motors in industrial applications," *Engineering Research Express*, vol. 6, p. 032304, 2024, doi: 10.1088/2631-8695/ad7d6b.
- [24] T. H. Atyia, "Various control strategies on Torque ripple minimization for switched reluctance motor," *IOP Conference Series: Materials Science and Engineering*, vol. 454, p. 012085, 2018, doi: 10.1088/1757-899X/454/1/012085.
- [25] H. He, X. Yao, J. Wang, B. Zheng, and Q. Guan, "Current optimized torque sharing function control for switched reluctance motor based on quasi-proportional resonance controller," *IEEE Journal of Emerging and Selected Topics in Power Electronics*, 2024, doi: 10.1109/JESTPE.2024.3519866.
- [26] M. Dowlatshahi, S. M. Saghaiannejad, J. W. Ahn, and M. Moallem, "Minimization of torque-ripple in switched reluctance motors over wide speed range," *Journal of Electrical Engineering and Technology*, vol. 9, no. 2, pp. 478–488, 2014, doi: 10.5370/JEET.2014.9.2.478.
- [27] S. Mahfoud, A. Derouich, A. Iqbal, and N. El Ouanjli, "ANT-colony optimization-direct torque control for a doubly fed induction motor: An experimental validation," *Energy Reports*, vol. 8, pp. 81–98, 2022, doi: 10.1016/j.egy.2021.11.239.
- [28] D. A. Torrey, X. M. Niu, and E. J. Unkauf, "Analytical modelling of variable-reluctance machine magnetization characteristics," *IEE Proceedings - Electric Power Applications*, vol. 142, no. 1, pp. 14–22, 1995, doi: 10.1049/ip-epa:19951567.

BIOGRAPHIES OF AUTHORS



Dhiyaa Mohammed Ismael    is from Iraq, Salahuddin Governorate. He obtained a Bachelor's degree in Electrical Engineering from the College of Engineering, Tikrit University, in 2015. After graduation, he worked in the private sector with companies specializing in electrical board manufacturing and generator control systems until 2022. In the same year, he started my Master's studies in Electrical Engineering at Tikrit University. He has completed the preparatory stage and is now in the research stage. He can be contacted at email: diyaa.z.khlail@st.tu.edu.iq.



Thamir Hassan Atyia    received the B.Eng. degree in Electrical and Electronics Engineering from the University of Technology, Iraq in 1988, the M.Phil. in Control System Engineering, from the University of Newcastle upon Tyne, United Kingdom in 1994, and Ph.D. in Control System Engineering from the University of Newcastle upon Tyne, United Kingdom in 1999. He is a member of the IET. Currently, he is an Associate Professor Lecturer in the Electrical Engineering Department, Tikrit University. He has over thirty years of experience in industry and academia as an engineer, educator, and administrator. He is well known as a technical leader in the machine control industry, a researcher in electric power engineering, an educator in engineering, and an administrator in higher education. His research interests cover: control and optimization, mathematical modeling and simulation, electrical machines, power systems, and renewable energy. He can be contacted at email: dr.thamir.atyia@tu.edu.iq.